RSC Advances

PAPER

View Article Online
View Journal | View Issue

Open Access Article. Published on 01 September 2015. Downloaded on 1/21/2026 7:33:29 PM.
This article is licensed under a Creative Commons Attribution 3.0 Unported Licence.

Cite this: *RSC Adv.*, 2015, **5**, 76133

Effective magnetic moment in cyclodextrin–polynitroxides: potential supramolecular vectors for magnetic resonance imaging†

F. Caglieris,[c] L. Melone,*[ab] F. Canepa,[d] G. Lamura,[c] F. Castiglione,[a] M. Ferro,[a] L. Malpezzi,[a] A. Mele,[a] C. Punta,[a] P. Franchi,[e] M. Lucarini,[e] B. Rossi[fg] and F. Trotta[h]

Received 23rd July 2015
Accepted 1st September 2015

DOI: 10.1039/c5ra14597j

www.rsc.org/advances

Nitroxides have great potential as contrast agents for Magnetic Resonance Imaging (MRI). Two β-cyclodextrin (βCD) derivatives bearing one or seven (2,2,6,6-tetramethylpiperidin-1-yl)oxyl (TEMPO) units on the small rim of βCD (**CD3** and **CD6** respectively) were synthesized. Their effective magnetic moments were measured by DC-SQUID magnetometry obtaining the values $\mu_{eff}/\mu_B \approx 1.7$ and $\mu_{eff}/\mu_B \approx 4.2$ for **CD3** and **CD6** respectively. Interestingly, while isothermal magnetization data of **CD3** were well described by a Brillouin function for a $S = 1/2$ single spin system, those associated with **CD6** could not be explained in the framework of a non-interacting spins model. For this reason, four different configurations for the seven interacting nitroxides were considered and modeled. The numerical results evidenced that only the configurations with a privileged central spin could take into account the experimental observations, thus justifying the reduced effective magnetic moment of **CD6**. The water relaxivity (r_1) in DMSO-d_6–water (9 : 1 v : v) solutions was also measured for both the derivatives obtaining the values $r_1 = 0.323$ mM^{-1} s^{-1} and $r_1 = 1.596$ mM^{-1} s^{-1} for **CD3** and **CD6** respectively.

1. Introduction

Persistent nitroxyl radicals (nitroxides) have found increasing applications in recent years in different important fields such as catalysts for oxidative processes,[1] for the development of materials for energy storage,[2] in molecular magnetism and spintronics.[3] Moreover, nitroxides have a promising future in the biomedical field. Indeed, they have been used for the synthesis of bio-compatible materials capable of protecting biological tissues from the damage caused by reactive oxygen species (ROS).[4] Due to their magnet-sensitive character, good cell membrane permeability and reduced toxicity, nitroxides are suitable spin-labels for *in vivo* Electron Spin Resonance (ESR) and Dynamic Nuclear Polarization (DNP) biological studies.[5] A very remarkable property of the nitroxides is their capability of decreasing the relaxation times (longitudinal T_1, and transversal, T_2) of water in biological tissues. For this reason they are currently investigated as MRI contrast agents (CA), suggesting their use as a potential alternative to the clinically used, but more toxic, gadolinium(III) complexes.[6] In general, the ability of a CA to enhance the proton relaxation rate ($1/T_{1,2}$, s^{-1}) is defined in terms of its relaxivity ($r_{1,2}$, mM s^{-1}) according to the eqn (1) where [CA] (mM) is the concentration of the CA and $1/T^0_{1,2}$ is the relaxation rate in absence of CA:

$$1/T_{1,2} = 1/T^0_{1,2} + r_{1,2}[\mathrm{CA}]. \quad (1)$$

Without going into the details of the Solomon–Bloembergen–Morgan theory of the paramagnetic relaxation,[7] the relaxivity of a CA is proportional to the square of its effective magnetic moment, μ_{eff}:

$$r_{1,2} = k\mu_{eff}^2 \quad (2)$$

However, several factors, mainly the solvent and the molecular structure of the CA, can significantly affect the proportionality constant (k), and thus the relaxivity value.[7] In order to be appealing in terms of imaging resolution, newly designed CA should be competitive with the present state-of-the-art

[a]Department of Chemistry, Materials and Chemical Engineering "G. Natta" Politecnico di Milano, Piazza L. Da Vinci 32, 20133 Milano, Italy. E-mail: lucio.melone@polimi.it
[b]Università Telematica e-Campus, Via Isimbardi 10, 22060 Novedrate, Como, Italy
[c]CNR-SPIN and Dipartimento di Fisica, Via Dodecaneso 33, 16146 Genova, Italy
[d]CNR-SPIN and Dipartimento di Chimica e Chimica Industriale, Via Dodecaneso 31, 16146 Genova, Italy
[e]Dipartimento di Chimica "G. Ciamician" Università di Bologna, Via San Giacomo 11, 40126 Bologna, Italy
[f]Elettra-Sincrotrone Trieste, Strada Statale 14 km 163.5, Area Science Park, 34149 Trieste, Italy
[g]Department of Physics, University of Trento, Via Sommarive 14, 38123 Povo, Trento, Italy
[h]Department of Chemistry, University of Torino, Via Pietro Giuria 7, 10125 Torino, Italy

† Electronic supplementary information (ESI) available. See DOI: 10.1039/c5ra14597j

Open Access Article. Published on 01 September 2015. Downloaded on 1/21/2026 7:33:29 PM.
This article is licensed under a Creative Commons Attribution 3.0 Unported Licence.

represented by Gd(III) complexes.[8] With its seven unpaired electrons, a Gd(III) ion has an effective magnetic moment of 7.94 μ_B (where μ_B is the Bohr magneton). Therefore the synthesis of new derivatives with an effective magnetic moment comparable or even higher than Gd(III) ion but less harmful to the human body is of high applicative interest. With regard to this aspect, the adoption of poly-nitroxides could be a valuable approach and significant contributions in this direction have been given by different investigators in the last years.[9]

Among the different compounds suitable for the creation of molecular architectures bearing poly-nitroxides, cyclodextrins (CDs) could represent a valid choice. Indeed, CDs are macrocyclic oligosaccharides composed by 6, 7, or 8 glucosidic units (α-, β- and γ-CD, respectively). These molecules are characterized by a truncated cone-shaped three-dimensional structure with an empty inner cavity having hydrophobic character. The hydroxyl groups of the anhydroglucose units are located both on the large rim (OH in position 2 and 3) and the small rim of the truncated cone (OH in position 6) (Fig. 1). Depending on their specific position, CDs' hydroxyl groups have different reactivity and a large number of methods for their selective chemical functionalization have been developed.[10] For this reason, CDs can be fruitfully applied for the synthesis of materials bearing multi-radical moieties.[11] Moreover, CDs have found relevant applications in the biomedical field as drug delivery systems due to their capability to form "host–guest" inclusion complexes both in solution and in the solid state with small molecules or portions of larger molecules.[12] Hence, in order to verify how CDs bearing nitroxyl radicals could be potentially attractive for possible application as CA for MRI, a detailed characterization of their magnetic properties is mandatory.

For this very reason, in this paper we present a detailed study on the magnetic properties of spin labelled CDs obtained by introducing TEMPO radical moieties onto βCD small rim *via* a click-chemistry approach (see Fig. 1). Both the mono-TEMPO (**CD3**) and the hepta-TEMPO (**CD6**) derivative have been synthesized and characterized. Their paramagnetic properties have been investigated by ESR spectroscopy and DC-SQUID magnetometry. The experimental results have been analysed and discussed on the basis of a standard quantum-statistical model. The longitudinal relaxivity of water, in presence of both **CD3** and **CD6**, and using DMSO as solvent has been measured and discussed as well.

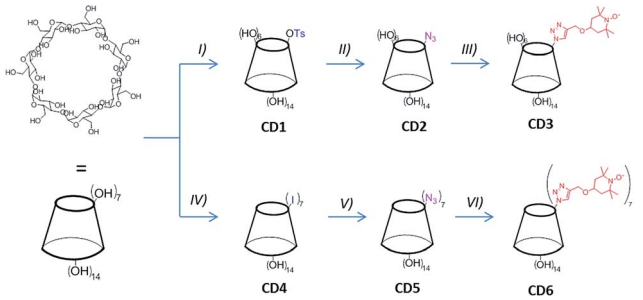

Fig. 1 Synthetic scheme. (I) TsCl, NaOH (aq.) 0.4 M, 0 °C 8 h; (II) NaN_3, DMSO, 90 °C, 12 h; (III) propargyl–TEMPO, DMF, CuI, Et_3N, 50 °C, 24 h; (IV) I_2, PPh_3, DMF, r.t., 18 h; (V) NaN_3, DMSO, 90 °C, 12 h; (VI) propargyl–TEMPO, DMF, CuI, Et_3N, 50 °C, 24 h.

2. Experimental

2.1. General

β-Cyclodextrin (βCD) and other reagents and solvents were commercially available and used as received unless otherwise stated. The synthesis of 6A-*O*-*p*-toluenesulfonyl-βCD (**CD1**) was performed following a published procedure with minor modifications as detailed in the ESI.†[21] The corresponding monoazide derivative (**CD2**) was obtained reacting **CD1** with an excess of NaN_3 in DMSO at 90 °C overnight (see ESI† for details). Heptakis-6-iodo-6-deoxy-βCD (**CD4**) and the corresponding azide (**CD5**) were synthesized as reported in literature.[13] Propargyl–TEMPO was obtained following the paper of Bogdan and McQuade.[22]

2.2. Synthesis of CD3 and CD6

CD3 was prepared by dissolving 1.160 g (1 mmol) of **CD2** in 5 mL of DMF containing 48 mg (0.25 mmol) of CuI and few drops of Et_3N in a two-necked flask (10 mL). The mixture was stirred under nitrogen atmosphere for 15 min at 50 °C. Then, 315 mg of propargyl–TEMPO (1.5 mmol) were added. After 24 h under the same conditions, the liquid mixture was concentrated under reduced pressure (1–1.5 mL final volume) and transferred into a chromatography column containing a silica-gel bed packed using DMF with a 30% ammonia aqueous solution (DMF : NH_4OH = 100 : 1, v : v) in order to remove the copper salts. The eluted **CD3**-containing DMF solution was finally concentrated under reduced pressure (10 mbar – thermal bath at 50 °C) until almost complete evaporation of the DMF. The addition of acetone (100 mL) allowed the precipitation of the product that was recovered by filtration on paper and washed with acetone (4 × 50 mL). An orange colored powder, soluble in DMSO and DMF, scarcely soluble in water, and insoluble in acetone, was obtained in quantitative yield. The TLC analysis (dissolving the product in DMF) was performed using silica-gel 60 F254 aluminium sheets (Merck) and 2-propanol : water : EtOAc : NH_4OH (5 : 3 : 1 : 0.5) solution as eluent (R_f: 0.56).

The reduced form of **CD3** (**CD3-H**) was obtained dissolving **CD3** (140 mg, 0.1 mmol) in 1 mL of DMSO and then adding an excess of phenylhydrazine. The mixture was stirred at r.t. for 4 h. The solution was finally poured in acetone. The white precipitate was filtered on paper and extensively washed with acetone. ^{1}H-NMR (DMSO-d_6 + D_2O, 500 MHz): δ = 7.98 (s, 1H, triazole ring), 5.10–4.79 (m, 7H, H-1), 4.77 (m, 1H, H-6′a), 4.66–4.56 (m, 1H, H-6′b), 4.49 (s, 2H, CH_2), 3.90 (t, 1H, H-5′), 1.89 (m, 2H, CH-eq), 1.27 (m, 2H, CH-ax), 1.08 (s, 6H, CH_3-eq), 1.04 (s, 6H, CH_3-ax).

The product **CD6** was obtained similarly to **CD3** (50 °C under N_2 for 24 h) starting from 350 mg (0.27 mmol) of **CD5** and 526 mg (2.50 mmol) of propargyl–TEMPO in DMF (2 mL), in presence of CuI (30 mg, 0.16 mmol) and Et_3N (3 drops). Purification was performed by column chromatography using silica-gel, first eluting with Hex : EtOAc (8 : 2) in order to remove the

 This journal is © The Royal Society of Chemistry 2015

Open Access Article. Published on 01 September 2015. Downloaded on 1/21/2026 7:33:29 PM.
This article is licensed under a Creative Commons Attribution 3.0 Unported Licence.

excess of propargyl–TEMPO and then with methanol for the recovery of the product. The evaporation of the solvent provided in quantitative yield an orange colored powder, soluble in $CHCl_3$, methanol, acetonitrile. TLC (silica-gel 60 F254, $CHCl_3$: MeOH 5 : 3) revealed one spot with R_f: 0.70. ^{1}H-NMR (DMSO-d_6 + phenylhydrazine + D_2O, 500 MHz): $\delta = 7.86$ (s, 1H, triazole ring), 5.08 (s, 7H, H-1), 1.78 (m, 14H, CH-eq), 1.18 (m, 14H, CH-ax), 1.04 (s, 42H, CH_3-eq), 1.00 (s, 42H, CH_3-ax).

2.3. Characterization

^{1}H, ^{13}C NMR, and ^{1}H–^{1}H TOCSY spectra of the products were recorded at 305 K with a Bruker Avance-500 MHz NMR spectrometer. The FT-IR solid phase spectra of the powdered sample with infrared grade KBr were recorded using a Varian 640-IR spectrometer. ESI-MS mass spectra were collected on a Bruker Esquire 3000+ with electrospray ionization source and ion-trap detector. The samples were analyses by direct infusion of suitable solutions in the spectrometer source. The peak assignment was supported by the simulation of the isotopic cluster of the corresponding molecular formula (see ESI†). EPR spectra were recorded at room temperature using an ELEXYS E500 spectrometer equipped with a NMR gaussmeter for the calibration of the magnetic field and a frequency counter for the determination of *g*-factors. Nitroxide concentrations were measured with respect to a solution of 2,2-diphenyl-1-picrylhydrazyl (DPPH) of known concentration using the signal from a ruby crystal as internal standard. Spectra were recorded by using the following instrument settings: microwave power 0.79 mW, modulation amplitude 0.04 mT, modulation frequency 100 kHz, scan time 180 s, 2k data points.

2.4. DC-SQUID magnetometry

Temperature dependent susceptibility and isothermal magnetization measurements have been performed by a commercial DC-SQUID magnetometer *MPMS Quantum Design* on mortar grinded powder samples.

2.5. Relaxivity measurements

The longitudinal relaxation time (T_1) measurements were performed on a 500 MHz Bruker Avance spectrometer by using a standard inversion–recovery (180–*t*–90) sequence. The time interval (*t*) was varied between 1 ms and 24 s (number of experiments NE = 22).

The repetition time was 40 s and the temperature was set at 305 K. Experiments were performed using a solution of DMSO-d_6–H_2O (9 : 1) with a specified concentration of **CD3** (3×10^{-2} to 3.3×10^{-3} mM) and **CD6** (7×10^{-2} to 7.7×10^{-3} mM) respectively. The integrals of the water peak in the ^{1}H spectra *vs.* the corresponding time *t*, were used to calculate the T_1 values by means of the supplied XWINNMR Bruker software, fitting the data with a mono-exponential function.

3. Results and discussion

3.1. TEMPO-CD synthesis

The synthesis of the mono-TEMPO-CD (**CD3**) and hepta-TEMPO-CD (**CD6**) is outlined in Fig. 1.

The Cu(I)-catalyzed cycloaddition between **CD2** and propargyl–TEMPO in DMF as solvent afforded the product **CD3** in quantitative yield. FT-IR analysis (Fig. SI13†) showed the disappearance of the azide characteristic peak (2100 cm^{-1}). ESI-MS analysis confirmed the presence of an intense peak associated to [**CD3** + Na]$^+$ at *m*/*z* 1392.9 (Fig. SI5†). The two very small peaks at *m*/*z* 1157.7 and *m*/*z* 1627.9 are associated respectively to the sodium cationized residual βCD and the **CD3** analogous with two nitroxide units attached. The NMR characterization was performed considering **CD3-H** obtained after reducing with phenylhydrazine the nitroxide radical of **CD3** to the corresponding hydroxylamine. The ^{1}H-NMR spectrum of **CD3-H** is reported in Fig. 2. The peaks assignment has been obtained from the corresponding ^{1}H–^{1}H TOCSY NMR spectrum reported in Fig. SI6.†

In order to obtain **CD6** we first synthesized the hepta-iodo derivative **CD4** following a classic procedure.[13] The substitution of the seven iodine atoms with azide afforded quantitatively the product **CD5**. Finally, propargyl–TEMPO units were attached to the derivative **CD5** providing the product **CD6** in quantitative yield. Also in this case, FT-IR analysis (Fig. SI13†) confirmed the complete disappearance of the azide peak. The ESI-MS analysis in positive mode and using methanol as solvent showed the presence of a small peak with *m*/*z* 2084.1 corresponding to [**CD6** + Na]$^+$, a very intense peak at *m*/*z* 1414.0 attributed to [**CD6** + 2Na]$^{2+}$ and close to a smaller peak associated to [**CD6** + H + Na]$^{2+}$ at *m*/*z* 1403.5. A small cluster at *m*/*z* 950.8 was also observed and attributed to [**CD6** + 3Na]$^{3+}$ (from Fig. SI8–12†). The NMR characterization of **CD6** was obtained by reducing the nitroxyl radicals with phenylhydrazine directly in the NMR tube and using DMSO-d_6 as solvent (see Fig. SI7†). The resolved spectrum showed the presence of a broad singlet at 5.08 ppm corresponding to the seven anomeric protons, and a multiplet in the region 6.0–5.8 ppm, assigned to the fourteen OH protons at the C2 and C3 positions of the anhydroglucose

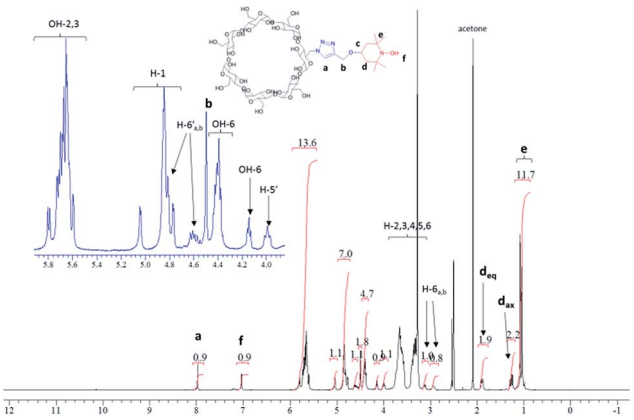

Fig. 2 ^{1}H-NMR spectrum of **CD3-H** in DMSO-d_6.

Open Access Article. Published on 01 September 2015. Downloaded on 1/21/2026 7:33:29 PM.
This article is licensed under a Creative Commons Attribution 3.0 Unported Licence.

unit. The latter assignment was confirmed by D_2O exchange (compare Fig. SI8b and c†). The βCD functionalization with seven TEMPO units was confirmed by the presence of the peaks associated to the piperidine ring, in particular the methyl groups (7 × 4) at 1.00 ppm, the $-CH_2-$ peaks as multiplets at 1.19 ppm (7 × 2, axial C–H) and 1.78 ppm (7 × 2, equatorial C–H) and the protons of the triazole groups as singlet at 7.86 ppm (7 × 1).

3.2. ESR spectroscopy

Fig. 3a shows the ESR spectrum of **CD3** (0.05 mM) recorded in water at room temperature. It is a three lines pattern spectrum similar to the one described by Lucarini *et al.* for an analogous derivative obtained from α-CD.[14] ESR spectrum of **CD6** (Fig. 3b) was recorded in acetonitrile at room temperature. It shows mainly one broad signal ($g = 2.0058$) whose integrated intensity corresponds quantitatively to the theoretical concentration of nitroxide units. The broadening (peak to peak line width 11.5 G) of the signal is independent of concentration, and thus inter-assembly interactions can be discounted. This spectrum is reminiscent of those obtained from very concentrated nitroxide solutions. Since it was obtained at 0.5 mM concentration, the signal broadening is ascribed to the proximity of spin centers of **CD6** within the framework of the cyclodextrin rim. This is consistent with exchange-coupled nitroxides with a coupling constant significantly larger than the ^{14}N hyperfine coupling, $|J/g\mu_B| \gg a(N)$ *i.e.*, $|J/k| \gg 2.0$ mK. The lack of resolved ESR multiplets should be attributed to the presence of many different transitions from different spin states arising from multiple interactions between the seven radical units. The spectrum shows also a very weak sharp satellite signals presumably due to some not-exchanging nitroxide units. However, theoretical simulation of the experimental spectrum indicated that these correspond to less than 0.5% of the total amount of nitroxide.[15]

3.3. Magnetic behavior of TEMPO-CD

The temperature dependence of the molar magnetic susceptibility for the **CD3** (a) and **CD6** (b) samples both measured under the form of grinded powders are shown in Fig. 4. Both the curves show a dominant paramagnetic behavior. In Fig. 5 the isothermal magnetization as a function of H/T at several temperatures from 2 up to 30 K is reported for **CD3** (a) and **CD6** (b), respectively. It is worth noticing that in the case of **CD3** all the experimental points collapse on the same line as expected for a system of non-interacting magnetic moments. Instead,

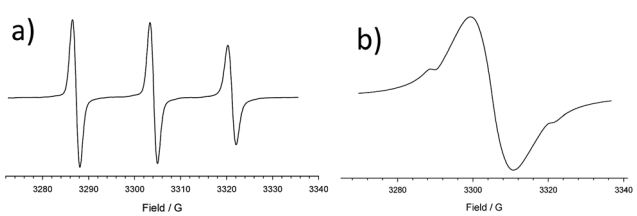

Fig. 3 ESR spectra of: (a) **CD3** (0.05 mM) in water at room temperature; (b) **CD6** (0.5 mM) in acetonitrile at room temperature.

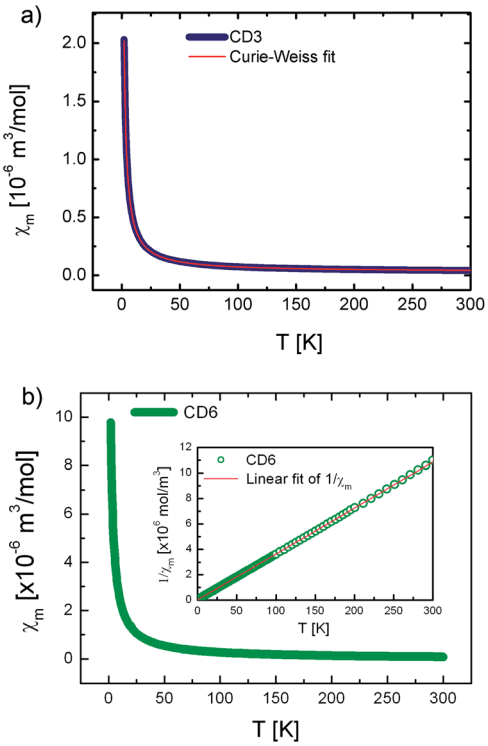

Fig. 4 Magnetic susceptibility as a function of temperature of (a) **CD3** and (b) **CD6** samples respectively. The experimental data were collected at $\mu_0 H = 0.05$ T. Standard or modified Curie–Weiss fits are reported as continuous lines (inset).

this is not the case for **CD6** whose behavior will be explained by taking into account antiferromagnetic (AFM) intra-molecular interactions (*vide infra*). The temperature dependent magnetic susceptibility was analyzed in the framework of a modified Curie–Weiss model (eqn (3)) where C is the Curie constant, θ the Curie–Weiss temperature and χ_0 is a temperature independent contribution.

$$\chi = \frac{C}{T - \theta} + \chi_0 \tag{3}$$

The obtained parameters for **CD3** and **CD6** are reported in Table 1. First, the T-independent term χ_0 is zero in the case of **CD6** while the positive value obtained for **CD3** was ascribed to an almost negligible ferromagnetic contribution. Since this spurious effect was indeed almost fully removed in a reference **CD3** sample precipitated from hot water, we ascribed it to a change of the molecular packing (data not shown).

A more relevant feature that emerges in both the samples is the existence of small and negative θ which indicates the presence of very weak AFM-like interactions. It is worth to notice that in case of **CD3** these interactions have inter-molecular origin while in **CD6** they are mainly due to intra-molecular exchange interactions as we will detail here below.

The 2 K **CD3** isothermal magnetization data reported in Fig. 6 was well fitted by a Brillouin function leaving S as free parameter.[16] We obtained $S = 0.452 \pm 0.001$ which confirms

 This journal is © The Royal Society of Chemistry 2015

Open Access Article. Published on 01 September 2015. Downloaded on 1/21/2026 7:33:29 PM.
This article is licensed under a Creative Commons Attribution 3.0 Unported Licence.

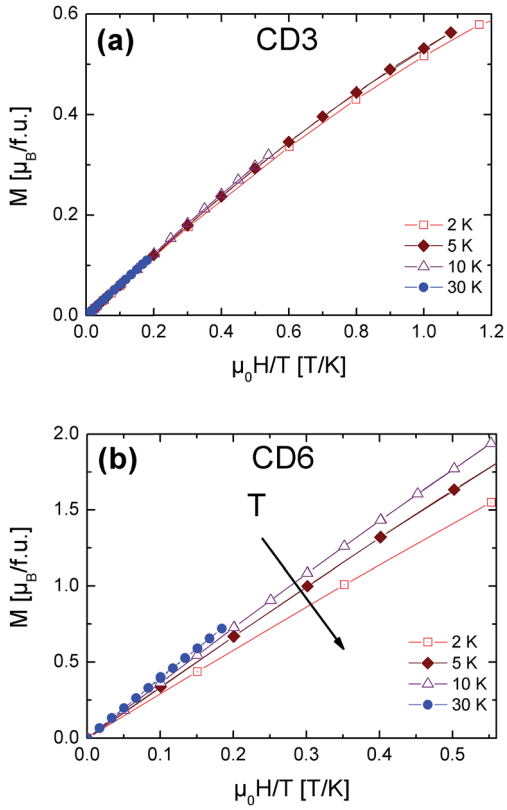

Fig. 5 CD3 (a) and CD6 (b) isothermal magnetization measurements as a function of H/T at different temperatures.

Table 1 Fit parameters of CD3 and CD6 χ_m curves. The effective magnetic moments μ_{eff} per molecules were extracted from the Curie constant[a]

Sample	C [10^{-6} m^3 K mol^{-1}]	θ [K]	χ_0 [10^{-6} m^3 mol^{-1}]	μ_{eff}/μ_B
CD3	4.471(1)	−0.240(4)	0.030(1)	1.686(1)
CD6	27.646(1)	−0.713(7)	0	4.193(1)

[a] $C = \mu_0 N_A \mu_{eff}^2/3k_B$ where N_A is the Avogadro's number, and k_B is the Boltzmann constant.

that **CD3** mono radical fully behaves as an ensemble of non-interacting spin $S = 1/2$. Indeed, the very small difference from the expected value $S = 1/2$ can be ascribed to the presence of tiny AFM inter-molecular interactions ($\theta < 0$ as reported in Table 1). The same figure also reports the experimental magnetization data of **CD6** at 2 K and the theoretical calculation for the case of a seven-non-interacting-spin-1/2 model. It is interesting to note that the rate $T\mathrm{d}M/\mathrm{d}H|_{H=0\,\mathrm{T}}$ is remarkably lower than the one expected for the non-interacting case. We ascribe this effect to the existence of non-negligible intra-molecular spin-interactions as we will detail hereafter. Firstly, we can safely exclude the presence of relevant inter-molecular interactions since the same result was obtained for a DMSO diluted sample (not shown).

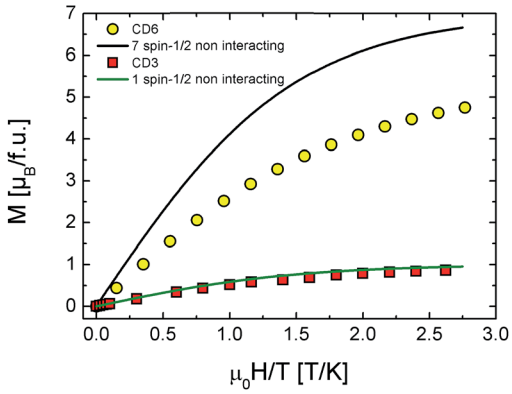

Fig. 6 Comparison between CD3 and CD6 magnetization data. The continuous lines represent a Brillouin function for a $S = 1/2$ non interacting spin ensemble and a model function for a system of seven-non-interacting $S = 1/2$ spins, for CD3 and CD6 respectively.

3.4. The spin interacting model

The failure of the non-interacting model in reproducing **CD6** experimental magnetization curve points out the necessity of including spin exchange interactions. In particular, we used a standard statistical approach to describe the case of hepta-radicals with intra-molecular interactions. All the theoretical calculations and fits have been implemented by home-made Mathematica 9.0 routines. Since the radicals can be imagined as equally spaced on CD rim, at first we considered a configuration of seven spins at the vertices of a regular heptagon (heptagonal-configuration) as shown in Fig. 7a with periodic boundary conditions ($S_{N+1} = S_1$) described by a Heisenberg-like Hamiltonian:[16]

$$H = -g\mu_B \sum_i \mu_0 \vec{H}\cdot\vec{S}_i - 2J_1 \sum_{\langle \mathrm{f.n.}\rangle} \vec{S}_i\cdot\vec{S}_j - 2J_2 \sum_{\langle \mathrm{s.n.}\rangle} \vec{S}_i\cdot\vec{S}_j \quad (4)$$

The first term represents the Zeeman contribution, the second and the third terms describes the coupling between first-neighbors (f.n.) and second-neighbors (s.n.) spins respectively with J_1 and J_2 representing the exchange integrals. Unfortunately, no reasonable choice of J_1 and J_2 parameters could successfully take into account our experimental data (see Fig. SI14†).

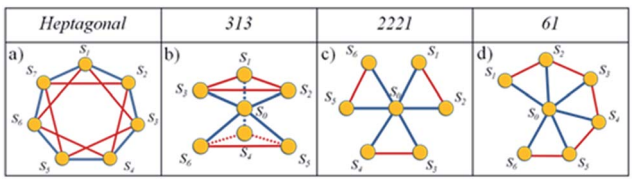

Fig. 7 Four different configurations for the seven radicals: (a) highly symmetric heptagonal configuration: the blue and red lines represent the J_1 and the J_2 coupling constants respectively. (b–d) In this case J_1 represent the exchange interaction between the central spin and the others ones whereas J_2 takes into account all other possible interactions excluding the central spin (see text for details).

Open Access Article. Published on 01 September 2015. Downloaded on 1/21/2026 7:33:29 PM.
This article is licensed under a Creative Commons Attribution 3.0 Unported Licence.

As second step we considered a less symmetric spin configuration with a fixed (central) spin with exchange interactions J_1 with its six neighbors (blue lines in Fig. 7b–d) and J_2 coupling between the other spin (red lines). In principle, this could be realized if one of the seven radicals is located into CD cavity and/or the whole molecule could be somehow distorted. In Fig. 7 we represent three different possible configurations, namely (b) **313**-, (c) **2221**- and (d) **61** as derived by following ref. 17.

The results of the analysis in the framework of our model are shown in Fig. 8 and summarized in Table 2. We note the following: (i) all the fitting functions are in very good agreement with experimental data. (ii) The values of the exchange integral J_1 and J_2 are both negative in all the configurations pointing to the AFM nature of the supposed intra-molecular interactions. (iii) They are of the same order of k_BT confirming the regime of weak coupling in which the Brillouin functions are not applicable.[16] (iv) J_1, J_2 values are in good agreement with the case of other multiradicals complex like calix[4]arene nitroxide tetraradicals.[18]

All these experimental evidences indicate that the existence of a *privileged spin* is crucial. This means that one of the radicals occupies the CD rim center and/or the molecule is somehow distorted to set a central spin. In both cases two types of AFM exchange interactions take place, the most intense (J_1) between one radical (the so called privileged- or central-spin) with the others and the less intense (J_2) between the other radicals. By concluding this section, DC magnetization measurements suggest the presence of effective intra-molecular exchange interactions between radicals that slightly reduces the effective magnetic moment per molecule down to 4.2 μ_B as deduced by a Curie–Weiss fit on temperature dependent susceptibility (see Fig. 4 and Table 1).

3.5. Relaxivity measurements

In view of the possible application for MRI of the proposed derivatives, the $1/T_1$ relaxation rates of water in **CD3** and **CD6** solutions in DMSO-d_6–H_2O (9 : 1) solutions at 305 K at different concentrations were measured. The associated water relaxivities (r_1) were calculated by fitting the data reported in Fig. 9 with eqn (1). For comparison, the same measurements were carried out considering also the derivative **4-OH-TEMPO** as model molecule. DMSO was chosen as solvent because both **CD3** and **CD6** were scarcely soluble in water. The relaxation rate increased in a linear fashion for all the compounds. The linear regression fitting provided the relaxivity values reported in Table 3. The relaxivity associated to **4-OH-TEMPO** is consistent with the value reported in literature (0.28 $mM^{-1}\ s^{-1}$, in phosphate buffer at 25 °C).[19] A slight increment of the relaxivity is observed with regard to the compound **CD3**. Probably, this effect could be associated to the higher molecular weight of **CD3** compared to **4-OH-TEMPO**. Indeed, it is reported that the water relaxivity increases with the molecular weight of the CA due to the slowing down of the molecular tumbling of the CA.[20] The order of magnitude of the relaxivity value of **CD6** is in line with those reported in literature for polynitroxyl functionalized dendrimers using acetonitrile-d_3/water solutions.[9b] According to the eqn (2), the relaxivity is proportional to the square of the effective magnetic moment. As the two derivatives **CD3** and **CD6** differ only for the number of TEMPO units onto the βCD upper rim, it is interesting to verify how this aspect affects the proportionality constant between r_1 and μ_{eff}^2. The ratio r_1(**CD6**)/r_1(**CD3**) = 4.94 is quite close to the ratio of the squared magnetic moments, μ_{eff}^2(**CD6**)/μ_{eff}^2(**CD3**) ≈ 6.19, but these values are not coincident. Thus, the inequality r_1(**CD6**)/r_1(**CD3**) < μ_{eff}^2(**CD6**)/μ_{eff}^2(**CD3**) is equivalent to k(**CD6**) < k(**CD3**) (see eqn (2)). This

Table 2 J_1 and J_2 values for **313**-, **2221**- and **61**-configuration of **CD6** calculated for $T = 2$ K

Configuration	J_1/k_BT	J_2/k_BT
313	−1.07	−0.47
2221	−1.06	−0.81
61	−1.07	−0.53

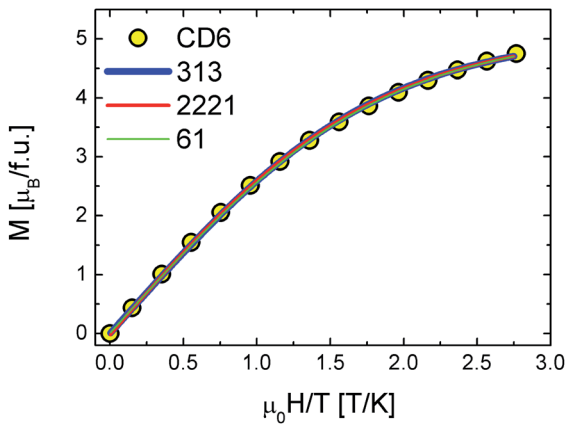

Fig. 8 **CD6** magnetization data *vs.* **313** (blue line), **2221** (red line) and **61** (green line) configuration model calculations.

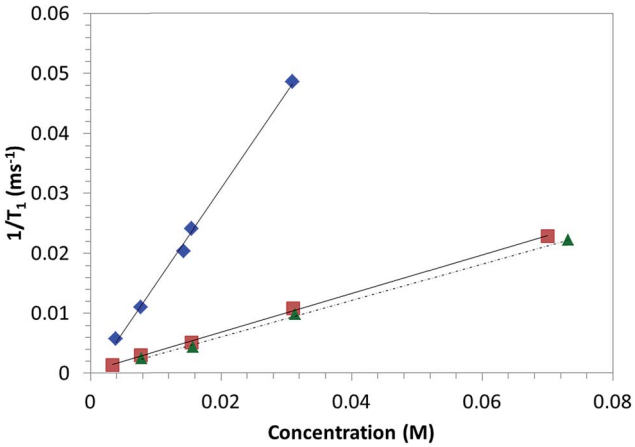

Fig. 9 Relaxation rates for **4-OH-TEMPO** (▲), **CD3** (■) and **CD6** (◆) in DMSO-d_6–H_2O (9 : 1) at 305 K.

Open Access Article. Published on 01 September 2015. Downloaded on 1/21/2026 7:33:29 PM.
This article is licensed under a Creative Commons Attribution 3.0 Unported Licence.

Table 3 ^{1}H r_1 relaxivity of water in DMSO-d_6–H_2O (9 : 1) solutions at 305 K

Compound	r_1 (mM^{-1} s^{-1})
4-OH-TEMPO	0.305
CD3	0.323
CD6	1.596

result is probably ascribed to an enhanced hydrophobicity of the derivative **CD6** compared to **CD3**, due to the reduced number of hydroxyl groups and the increased number of TEMPO units in **CD6**. The structural differences between **CD3** and **CD6** are expected, in turn, to affect parameters such as the number of inner-sphere bound water molecules and the correlation time, factors concurring to the overall values of k.[7]

In conclusion, if from one side the introduction of more TEMPO units on the βCD molecule positively affects the relaxivity by increasing the effective magnetic moment of the CA, from another side it leads to a modification of the interactions between the water molecules and the CA, causing a small, but not negligible, reduction of the water relaxivity values.

Finally, we would like to add a note about the reduced solubility in water of the proposed derivatives **CD3** and **CD6**. Despite water soluble molecules are required for the applications, this aspect is not crucial in the present work. Instead, it is aimed mainly at investigating how the number of TEMPO radical units onto the βCD molecule affects the magnetic behavior of the corresponding derivative. The interesting results obtained so far strengthen the validity of the methodological approach followed in this work that does not depend on the effective solubility in water of the compounds. With regard to this point, **CD3** and **CD6** should be considered as model molecules rather than final derivatives for a direct application. However, a future development of the work is certainly oriented towards the synthesis and characterization of cyclodextrin–polynitroxides with increased solubility in biological media.

4. Conclusions

In summary, two βCD derivatives bearing one or seven TEMPO radical units (**CD3** and **CD6** respectively) on the small rim of the βCD molecule have been synthesized and characterized. Their effective magnetic moments have been measured by DC-SQUID magnetometry. While isothermal magnetization data of **CD3** are well fitted by a Brillouin function for $S = 1/2$ single spin system, those associated to **CD6** cannot be simply described in the framework of a non-interacting spins model. In order to fully understand **CD6** experimental data, four different configurations for the seven interacting free-radicals, with or without the presence of a central spin, have been considered and modeled. The numerical results evidences that only the configurations with a *privileged* central spin fully takes into account the experimental behavior justifying a reduced effective magnetic moment. The effective magnetic moments μ_{eff} of both the derivatives were determined from dc susceptibility measurements obtaining the values $\mu_{eff}/\mu_B = 1.686$ and $\mu_{eff}/\mu_B = 4.193$ for **CD3** and **CD6** respectively.

Considering the envisaged application of the proposed βCD-TEMPO derivatives as macromolecular building blocks for nitroxides-based MRI contrast agents, we studied the NMR relaxivities (r_1) in DMSO-d_6–water (9 : 1 v : v) solutions. The values $r_1 = 0.323$ mM^{-1} s^{-1} and $r_1 = 1.596$ mM^{-1} s^{-1} for **CD3** and **CD6** respectively were obtained. Interestingly, the values associated to **CD6** is not too far from Gd-based CA relaxivity.[6i] Taking into account the well-known reduced toxicity of TEMPO radicals, βCD bearing multiple TEMPO moieties can be surely considered as promising MRI and ESR CA for *in vivo* experiment. For this reason, future efforts will be devoted to the synthesis of analogous water-soluble derivatives.

Contributions

L. Me. contributed to the synthetic part. F. Cg., F. Cn. and G. L. carried out the magnetic measurements, and analyzed the data by a quantum-statistical model. F. C., M. F. and A. M. performed the relaxivity measurements. P. F. and M. L. performed the ESR spectroscopy measurements. All the coauthors contributed to the analysis and the interpretation of the data. L. Me., F. Cg. and G. L. wrote the manuscript, with the support of all the coauthors.

Acknowledgements

The Ministry for Education, University and Research (MIUR) is kindly acknowledged through the following Research Projects: PRIN 2010-2011-NANOMED, PRIN-2010-2011-PROxi project 2010PFLRJR_005, and PRIN MULTINANOITA.

Notes and references

1 (*a*) S. Wertz and A. Studer, *Green Chem.*, 2013, **15**(11), 3116–3134; (*b*) B. L. Ryland and S. S. Stahl, *Angew. Chem., Int. Ed.*, 2014, **53**, 8824–8838.
2 (*a*) Z. Song and H. Zhou, *Energy Environ. Sci.*, 2013, **6**, 2280–2301; (*b*) F. Behrends, H. Wagner, A. Studer, O. Niehaus, R. Pöttgen and H. Eckert, *Macromolecules*, 2013, **46**, 2553–2561.
3 N. M. Gallagher, A. Olankitwanit and A. Rajca, *J. Org. Chem.*, 2015, **80**, 1291.
4 (*a*) T. Yoshitomi, A. Hirayama and Y. Nagasaki, *Biomaterials*, 2011, **32**(31), 8021–8028; (*b*) T. Yoshitomi, Y. Yamaguchi, A. Kikuchi and Y. Nagasaki, *Acta Biomater.*, 2012, **8**, 1323–1329.
5 (*a*) F. Hyodo, S. Matsumoto, N. Devasahayam, C. Dharmaraj, S. Subramanian, J. B. Mitchell and M. C. Krishna, *J. Magn. Reson.*, 2009, **197**, 181–185; (*b*) M. C. Emoto, H. Sato-Akaba, H. Hirata and H. G. Fujii, *Free Radical Biol. Med.*, 2014, **74**, 222–228; (*c*) C. Sauve, M. Rosay, G. Casano, F. Aussenac, R. T. Weber, O. Ouari and P. Tordo, *Angew. Chem., Int. Ed.*, 2013, **52**, 10858–10861; (*d*) E. Elisei, M. Filibian, P. Carretta, S. Colombo Serra, F. Tedoldi, J. F. Willart, M. Descamps and A. Cesàro, *Chem. Commun.*, 2015, **51**, 2080.

Open Access Article. Published on 01 September 2015. Downloaded on 1/21/2026 7:33:29 PM.
This article is licensed under a Creative Commons Attribution 3.0 Unported Licence.

6 (*a*) Z. Zhelev, R. Bakalova, I. Aoki, K. Matsumoto, V. Gadjeva, K. Anzai and I. Kanno, *Mol. Pharm.*, 2009, **6**(2), 504–512; (*b*) Z. Zhelev, R. Bakalova, I. Aoki, K.-I. Matsumoto, V. Gadjeva, K. Anzai and I. Kanno, *Chem. Commun.*, 2009, 53–55; (*c*) Z. Zhelev, V. Gadjeva, I. Aoki, R. Bakalova and T. Saga, *Mol. BioSyst.*, 2012, **8**, 2733–2740; (*d*) E. J. Rivera, R. Sethi, F. Qu, R. Krishnamurthy, R. Muthupillai, M. Alford, M. A. Swanson, S. S. Eaton, G. R. Eaton and L. J. Wilson, *Adv. Funct. Mater.*, 2012, **22**, 3691–3698; (*e*) A. L. Kleschyov, V. Sen', V. Golubev, K. Münnemann, D. Hinderberger, K. J. Lackner, S. Weber, M. Terekhov, L. M. Schreiber and T. Münzel, *Eur. J. Med. Chem.*, 2012, **58**, 265–271; (*f*) A. Rajca, Y. Wang, M. Boska, J. T. Paletta, A. Olankitwanit, M. A. Swanson, D. G. Mitchell, S. S. Eaton, G. R. Eaton and S. Rajca, *J. Am. Chem. Soc.*, 2012, **134**, 15724–15727; (*g*) Z. Zhelev, R. Bakalova, I. Aoki, D. Lazarova and T. Saga, *ACS Chem. Neurosci.*, 2013, **4**, 1439–1445; (*h*) M. Soikkeli, K. Sievanen, J. Peltonen, T. Kaasalainen, M. Timonen, P. Heinonen, S. Rönkkö, V.-P. Lehto, J. S. Kavakka and S. Heikkinen, *RSC Adv.*, 2015, **5**, 15507; (*i*) M. Rohrer, H. Bauer, J. Mintorovitch, M. Requardt and H.-J. Weinmann, *Invest. Radiol.*, 2005, **40**(11), 715–724.

7 (*a*) É. Tóth, L. Helm and A. E. Merbach, Contrast agents I, Magnetic Resonance Imaging, in *Topics in Current Chemistry*, ed. W. Krause, Springer, 2002, vol. 221, pp. 62–98; (*b*) É. Tóth, L. Helm and A. E. Merbach, in *The chemistry of contrast agents in medical magnetic resonance imaging*, ed. L. Helm, A. E. Merbach and É. Tóth, Wiley, 2nd edn, 2013, pp. 25–76.

8 (*a*) S. Aime, C. Cabella, S. Colombatto, S. Geninatti Crich, E. Gianolio and F. Maggioni, *J. Magn. Reson. Imag.*, 2002, **16**, 394–406; (*b*) S. Aime, S. Geninatti Crich, E. Gianolio, G. B. Giovenzana, L. Tei and E. Terreno, *Coord. Chem. Rev.*, 2006, **250**, 1562–1579.

9 (*a*) A. Rajca, M. Pink, T. Rojsajjakul, K. Lu, H. Wang and S. Rajca, *J. Am. Chem. Soc.*, 2003, **125**, 8534–8538; (*b*) A. J. Maliakal, N. J. Turro, A. W. Bosman, J. Cornel and E. W. Meijer, *J. Phys. Chem. A*, 2003, **107**, 8467–8475; (*c*) O. Zeika, Y. Li, S. Jockusch, G. Parkin, A. Sattler, W. Sattler and N. J. Turro, *Org. Lett.*, 2010, **12**(16), 3696–3699; (*d*) A. Olankitwanit, V. Kathirvelu, S. Rajca, G. R. Eaton, S. S. Eaton and A. Rajca, *Chem. Commun.*, 2011, **47**, 6443–6445; (*e*) E. L. Dane, B. Corzilius, E. Rizzato, P. Stocker, T. Maly, A. A. Smith, R. G. Griffin, O. Ouari, P. Tordo and T. M. Swager, *J. Org. Chem.*, 2012, **77**, 1789–1797; (*f*) M. F. Ottaviani, A. Modelli, O. Zeika, S. Jockusch, A. Moscatelli and N. J. Turro, *J. Phys. Chem. A*, 2012, **116**, 174–184; (*g*) M. Porel, M. F. Ottaviani, S. Jockusch, N. J. Turro and V. Ramamurthy, *RSC Adv.*, 2013, **3**, 427–431.

10 (*a*) A. R. Khan, P. Forgo, K. J. Stine and V. T. D'Souza, *Chem. Rev.*, 1998, **98**, 1977–1996; (*b*) F. Bellia, D. La Mendola, C. Pedone, E. Rizzarelli, M. Saviano and G. Vecchio, *Chem. Soc. Rev.*, 2009, **38**, 2756–2781.

11 (*a*) V. Chechik and G. Ionita, *Org. Biomol. Chem.*, 2006, **4**, 3505–3510; (*b*) V. Chechik and G. Ionita, *New J. Chem.*, 2007, **31**, 1726–1729; (*c*) G. Ionita and V. Chechik, *Chem. Commun.*, 2010, **46**, 8255–8257; (*d*) G. Ionita, A. M. Ariciu, I. M. Turcu and V. Chechik, *Soft Matter*, 2014, **10**, 1778.

12 K. Hattori and H. Ikeda, in *Cyclodextrins and Their Complexes*, ed. H. Dodziuk, Wiley, 2006, pp. 31–64.

13 P. R. Ashton, R. Königer and J. F. Stoddart, *J. Org. Chem.*, 1996, **61**(3), 903–908.

14 C. Casati, P. Franchi, R. Pievo, E. Mezzina and M. Lucarini, *J. Am. Chem. Soc.*, 2012, **134**, 19108–19117.

15 P. Franchi, E. Mezzina and M. Lucarini, *J. Am. Chem. Soc.*, 2014, **136**, 1250.

16 A. Rajca, *Chem. Rev.*, 1994, **94**, 871.

17 E. Belorizky and P. H. Fries, *J. Chim. Phys.*, 1993, **90**, 1077.

18 A. Rajca, S. Mukherjee, M. Pink and S. Rajca, *J. Am. Chem. Soc.*, 2006, **128**(41), 13497–13507.

19 E. Tanimoto, S. Karasawa, S. Ueki, N. Nitta, I. Aoki and N. Koga, *RSC Adv.*, 2013, **3**, 3531.

20 K. N. Raymond and V. C. Pierre, *Bioconjugate Chem.*, 2005, **16**, 3–8.

21 B. Brady, N. Lynam, T. O'Sullivan, C. Ahern and R. Darcy, *Org. Synth.*, 2000, **77**, 220.

22 A. Bogdan and D. T. McQuade, *Beilstein J. Org. Chem.*, 2009, **5**, 17, DOI: 10.3762/bjoc.5.17.

 This journal is © The Royal Society of Chemistry 2015